Climate Dynamics
https://doi.org/10.1007/s00382-023-06898-1

The impact of a uniform ocean warming on the West African monsoon

Harry Mutton[1] · Robin Chadwick[2] · Matthew Collins[1] · F. Hugo Lambert[1] · Christopher M. Taylor[3,4] · Ruth Geen[5] · Alexander Todd[1]

Received: 13 September 2022 / Accepted: 15 July 2023

Abstract
Projections of West African Monsoon (WAM) precipitation are uncertain. To address this, an improved understanding of the mechanisms driving WAM precipitation change is needed to shed light on inter-model differences and aid model development. The full forcing of increased CO_2 can be decomposed into different components such as the impact of ocean warming, or the direct radiative effect of increased CO_2. This paper investigates such a decomposition, analysing the effect of a uniform 4K ocean warming whilst keeping atmospheric CO_2 concentrations constant. The analysis highlights several mechanisms acting to decrease WAM precipitation over a range of timescales, from days after the abrupt ocean warming, to the long-term equilibrium response. The initial decrease in WAM precipitation is caused by warming and enhanced convection over the ocean, stabilising the atmosphere inland and disrupting the monsoon inflow at low levels. Later in the response (after about 5 days), the WAM precipitation is reduced through a strengthening of the shallow circulation over West Africa, associated with changes in the large-scale temperature gradients and a local warming of the atmosphere related to a soil moisture feedback mechanism over the Sahel. Finally, from around 20 days after the SST increase, the WAM precipitation is also reduced through changes in specific humidity gradients that lead to increased potency of dry air advection into the monsoon rainband. The analysis concludes by demonstrating that the processes affecting precipitation in the early stages of the response are also relevant to the long-term equilibrium response.

Keywords Africa · Monsoons · Atmosphere · Climate change

1 Introduction

Beginning in early May and reaching a peak intensity around August, the West African Monsoon (WAM) is responsible for the precipitation that falls during the summer months over West Africa (Cook and Vizy 2019; Zhang and Cook 2014; Akinsanola and Zhou 2020). Millions of people depend on rainfall supplied by the WAM, which is crucial for supporting agriculture in the region. Alongside this, much of the population relying on the monsoon have a relatively low adaptive capacity (Busby et al. 2014; Cook and Vizy 2019; Raj et al. 2019). Reliable rainfall projections are therefore vital for developing well-informed adaptation strategies that can support this climate-vulnerable population. Despite this, long term climate model projections of the WAM precipitation are uncertain (Raj et al. 2019; Wang et al. 2020; Gaetani et al. 2017). The Working Group I Contribution to the Sixth Assessment Report of the Intergovernmental Panel on Climate Change (Masson-Delmotte et al. 2021) state with only medium confidence that "precipitation is projected to increase over the central Sahel and decrease over the far western Sahel". Within the CMIP6 model ensemble, there are coupled models that predict both large increases and decreases in WAM precipitation in response to an abrupt quadrupling of CO_2 (see Fig. 1). To address this, it has been suggested that an improved understanding of the key mechanisms leading to precipitation change can help identify the inter-model differences at the root of the large uncertainty in WAM precipitation projections (Chadwick et al. 2017).

✉ Harry Mutton
hm580@exeter.ac.uk

1 University of Exeter, Exeter, UK

2 Global Systems Institute, University of Exeter and Met Office Hadley Centre, Exeter, UK

3 UK Centre for Ecology and Hydrology, Wallingford, UK

4 National Centre for Earth Observation, Wallingford, UK

5 University of Birmingham, Birmingham, UK

Published online: 29 July 2023

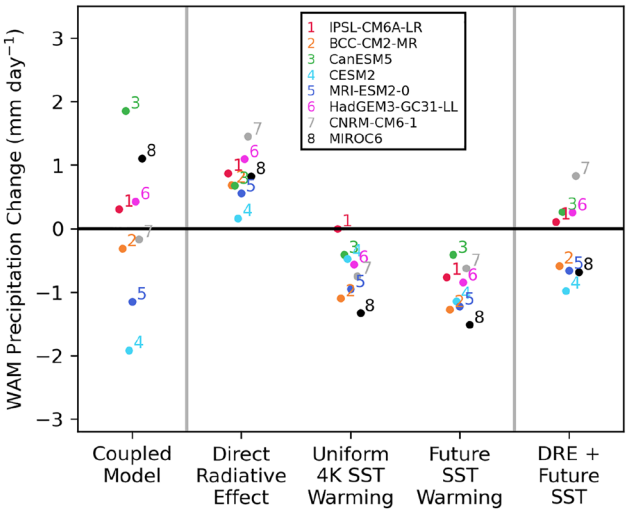

Fig. 1 West African Monsoon precipitation response across 8 CMIP6 GCMs; Coupled GCM (comparing years 50–150 in the abrupt-4xCO2 and piControl experiments), Direct Radiative Effect (amip-4xCO2 - amip), Uniform 4K SST Warming (amip-p4K - amip), Future SSTs (amip-future4K - amip), and DRE + Future SSTs (referring to the sum of the precipitation response to the Direct Radiative Effect and Future SST warming). WAM precipitation is defined as the area average precipitation over the dashed blue box indicated in Fig. 4b between June–August. See Appendix 1 for a description of the different CMIP6 experiments used to produce this decomposition

Using Atmosphere-only General Circulation Models (AGCM)s, the full forcing of increased atmospheric CO_2, simulated using coupled GCMs, can be broken down into a number of direct and indirect effects (Chadwick et al. 2017, 2019). Performing such a decomposition can simplify the coupled model response to increased CO_2. We suggest that by understanding each driver individually, it is possible to gain an improved understanding of the mechanisms that lead to precipitation changes in the coupled GCM simulations. A plot of the precipitation response to different forcing experiments (see Appendix 1) across a range of CMIP6 models can be seen in Fig. 1. Here, the coupled model response refers to the full forcing of increased CO_2, and the different components of this full response are highlighted in the columns following. One of these components is the indirect effect of a uniform SST warming (referring to the effect of uniformly warming the SSTs by 4K whilst keeping CO_2 concentrations constant). Figure 1 indicates that this uniform 4K ocean warming causes a decrease in WAM precipitation in a range of CMIP6 models, a response consistent with the findings of Gaetani et al. (2017) and Held et al. (2005). The direct radiative effect refers to the impact of increasing atmospheric CO_2 concentrations whilst keeping SSTs fixed. Figure 1 indicates that the direct radiative effect causes an increase in WAM precipitation, consistent with the results of Mutton et al. (2022) and Gaetani et al. (2017). The future SST warming column refers to the impact of a non-uniform ocean warming whilst keeping CO_2 concentrations constant, aiming to reflect a projected SST pattern in a future climate with increased atmospheric CO_2 concentrations. The global mean SST perturbation in the future SST column is 4K and can therefore be thought of as the Uniform SST warming with an additional pattern applied. It is shown that similar to the uniform SST warming, this also causes a decrease in WAM precipitation. Using these AGCM experiments to decompose the coupled model response could provide useful insight into the intermodel differences in the coupled models by exploring relevant physical mechanisms.

It has previously been shown that in CMIP5 models the different components of this decomposition add up fairly linearly to produce the full coupled response (Chadwick et al. 2017). In Fig. 1 however, the sum of the direct radiative effect and the future SST experiments are not always equal to the coupled response. To produce the coupled response using this kind of decomposition, the AGCMs must be forced by SSTs from the respective coupled model (Chadwick et al. 2017; Skinner et al. 2012). Such a decomposition has been produced using "timeslice" experiments (see Appendix 1) Chadwick et al. (2017). To demonstrate the linearity of this decomposition, maps showing the sum of the "timeslice" decomposition components, the coupled model response, and the difference between the two have been shown in Fig. 2. Here, the sum of the components performs well in capturing the coupled model response and the residual term is small. This result suggests that using such a decomposition can be useful in understanding the coupled model response. The reason these timeslice experiments have not been used throughout the analysis is due to the small number of models that have run them (4).

A decomposition as seen in Fig. 1 has been used previously in an investigation into the impact of the direct radiative effect on the WAM. Mutton et al. (2022) highlighted several key mechanisms that lead to an increase in precipitation. It was shown that a weakening of the shallow meridional circulation over West Africa caused a reduction in dry air advection into the monsoon rainband and an increase in monsoon precipitation (see schematic in Fig. 3). These circulation changes were shown to be generated through changes in large-scale temperature gradients (caused by differing constraints on atmospheric temperature between the dry desert airmass and the moist monsoon airmass) as well as local soil moisture feedbacks over the Sahel which lead to a local enhancement of these large-scale gradients in temperature.

Investigating the impact of a uniform ocean warming, it has been found that in general the tropic-wide response is for precipitation to increase over the ocean and to decrease over many land regions (Chadwick et al. 2019; He et al. 2014). Looking more specifically at the WAM, previous work has demonstrated that in response

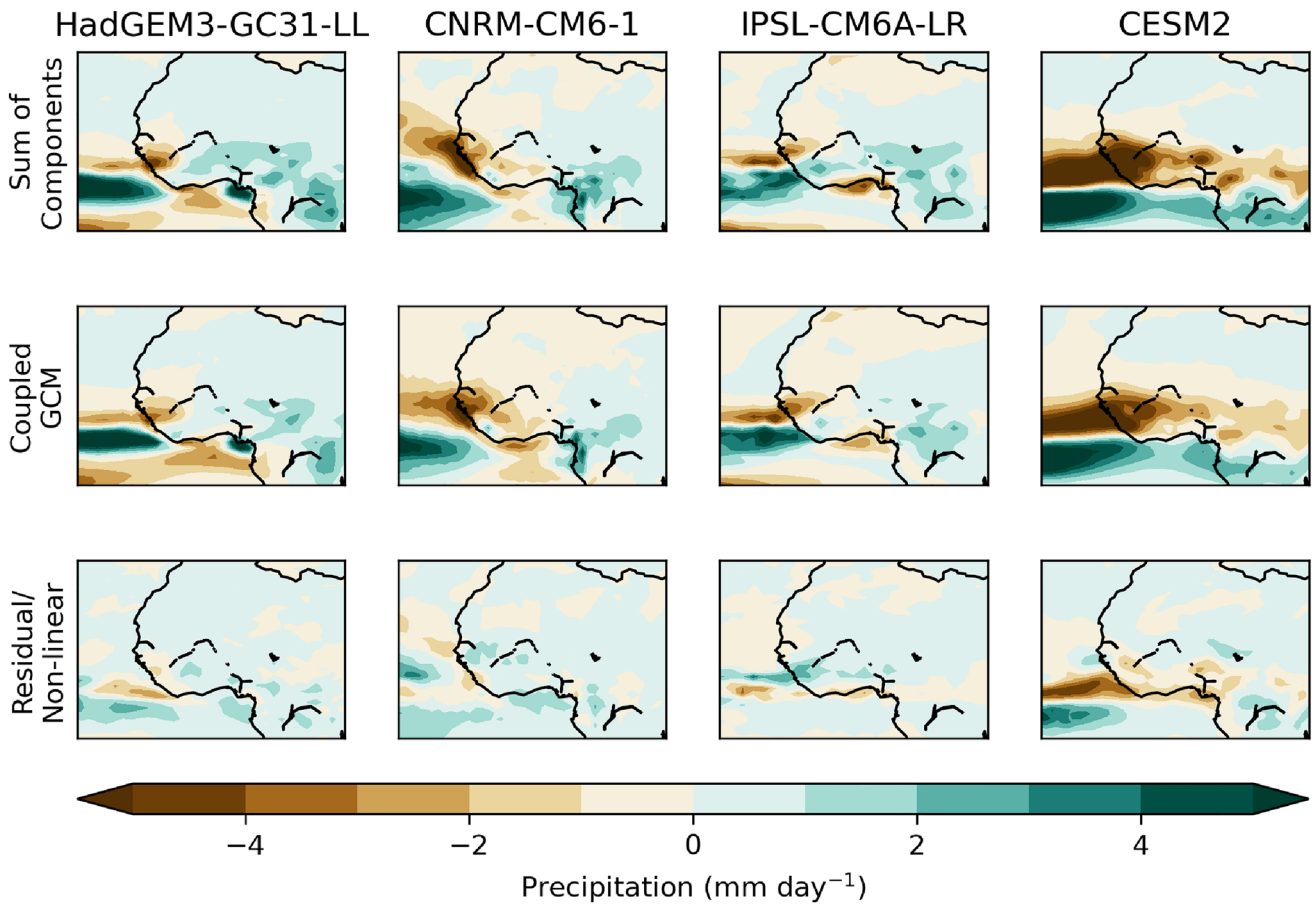

Fig. 2 Maps of anomalous JJA precipitation from the sum of the timeslice decomposition (see Appendix 1), the coupled model response (abrupt-4xCO2 - piControl), and the difference between the two, highlighting the non-linear processes not captured in the timeslice decomposition

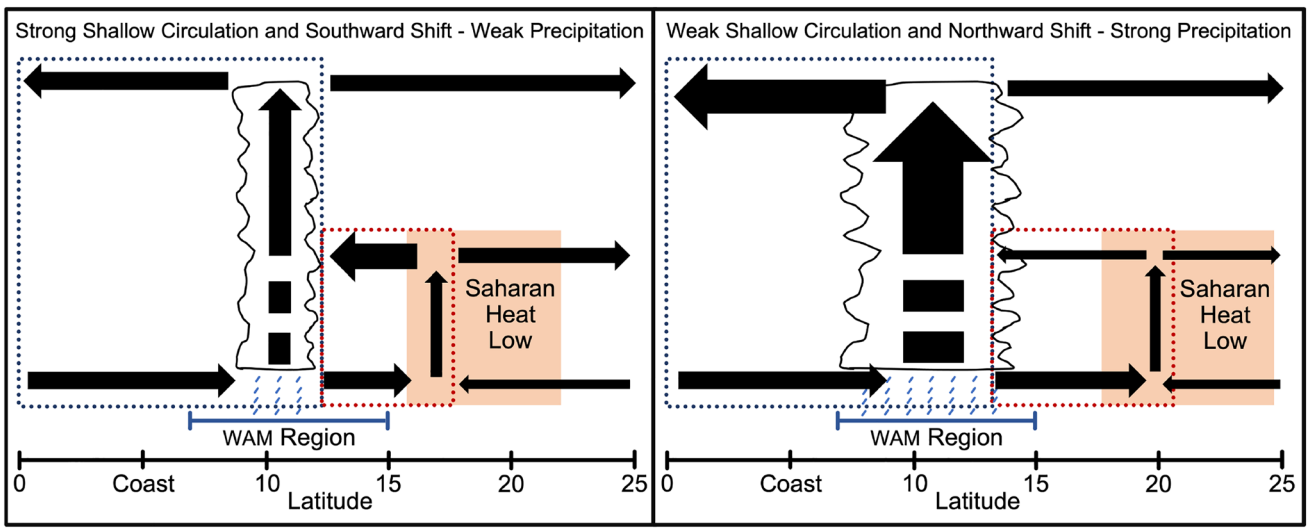

Fig. 3 Schematics depicting the climatological circulation over West Africa during the monsoon season and the relationship between the shallow circulation and monsoon precipitation (Shekhar and Boos 2017). Deep circulation highlighted by blue dotted box and shallow circulation indicated by red dotted box. Strong (weak) and southward (northward) shifted shallow circulation associated with weaker (stronger) monsoon precipitation

to a uniform ocean warming, the WAM precipitation decreases (Mutton et al. 2022; Gaetani et al. 2017; Held et al. 2005; Hill et al. 2017; Biasutti 2013, 2019; Giannini et al. 2003, 2008).

A number of different mechanisms have been suggested for drying the WAM in response to uniform ocean warming, but their relative importance and interactions with each other remain unclear. Gaetani et al. (2017) describe how the WAM precipitation is reduced through a heating of the troposphere that increases stability inland as in Caminade and Terray (2010), and through a general weakening of the monsoon circulation. This is consistent with the results of Giannini (2010) who describe how ocean warming imposes stability and reduces convection over land. Held et al. (2005) also identified a reduction in WAM precipitation in response to a uniform ocean warming, noting an impact of soil moisture on precipitation responses under warming. A soil moisture feedback was identified by Mutton et al. (2022) when investigating the direct radiative effect of increased CO_2 on the WAM. There, the feedback acted to amplify the precipitation response through changing soil moisture leading to anomalous surface heat fluxes which then influenced circulation changes. Hill et al. (2017) attributed the WAM response to ocean warming to enhanced moist static energy gradients in the mid-troposphere over the Sahel (10–20° N) which increase the advection of low moist static energy into the monsoon rainband. They showed that the increase in horizontal advection of low moist static energy is balanced by a decrease in vertical motion in the rainband, thus inhibiting precipitation. Each of these findings provide useful insight into the mechanisms that cause a reduction in WAM precipitation in response to a uniform SST increase. However, since these have only been demonstrated in the long-term 'equilibrium response', where the atmosphere has reached a steady state, it is not clear how this final state is reached or how the different mechanisms interact with each other.

This paper uses an ensemble of spin-up experiments in which an abrupt SST increase of 4K is applied. The response over the 30 days following this warming is analysed, helping to reveal the order in which different mechanisms affect WAM precipitation. It is then shown how the equilibrium response to the SST warming is reached and how the processes uncovered in the spin-up experiments are relevant to the longer-term response.

Section 2 describes the data and methods used in this analysis. Section 3 presents the results, looking at the response on the first day of the spin-up experiment, the transition throughout the spin-up response towards the equilibrium response, and the equilibrium response. Section 4 summarises the results and Sect. 5 presents a discussion, conclusions and some suggestions for future work.

2 Data and methods

2.1 Models

Most of the analysis presented in this paper makes use of HadGEM2-A, a CMIP5 AGCM with a resolution of 1.85° longitude by 1.25° latitude and 38 vertical levels output to 17 pressure levels. Further description can be found in Martin et al. (2011). HadGEM2-A is used since it enables the analysis of spin-up experiments not part of the CMIP6 model set.

An ensemble of 8 CMIP6 AGCMs is also used to compare the long term equilibrium response in HadGEM2-A to other models. The set of CMIP6 models used are those shown in Fig. 1: CESM2, BCC-CM2-MR, CNRM-CM6-1, HadGEM3-GC31-LL, IPSL-CMA6A-LR, MRI-ESM2-0, CanESM5, and MIROC6.

2.2 Experiment design

The analysis presented uses three experiments based on the atmosphere model intercomparison project. The control experiment (amip) uses prescribed monthly-varying SSTs and atmospheric constituents set to historical values. The two other experiments (amip-p4K and amip-p4K-spinup) use the same experimental setup with an additional 4K warming uniformly applied to the SSTs.

For the CMIP6 models, data is used between 1979 and 2014. For the HadGEM2-A experiments, seven ensemble members each initiated with different atmospheric state and soil moisture conditions (obtained from the CMIP5 HadGEM2-A r1i1p1 amip experiment on the 1st of August 1986, 1988, 1990, 1992, 1994, 1996, and 1998) are used. This ensemble runs with prescribed historical SSTs and atmospheric constituents from August 1986 to December 1998 for both the amip and amip-p4K experiment meaning the only difference between ensemble members is the initial conditions. The mean difference between amip and amip-p4K experiments provides the 'equilibrium' response to a uniform SST warming.

The amip-p4K-spinup analysis uses a similar experimental design. Here the term "spin-up" is used to describe the period immediately following the abrupt change in ocean temperatures. This captures the "spin-up" period from the initial amip state towards the long term steady state with uniform ocean warming. On the 1st of August 1988, 1990, and 1997 the spin-up experiment branches from the amip experiment. On these dates, the 4K uniform SST warming is applied and the model is run forward until December that year (Todd 2018). The days following the uniform warming are analysed using daily output from

these spin-up experiments. Treating each spin-up branch as its own ensemble member, a 21 member ensemble is obtained across the seven original amip runs and the three spin-up branches. To enable direct comparison, the same dates as the spin-up branches are used to investigate the equilibrium response. The HadGEM2-A experiments used here were originally designed for work not related to the WAM. Therefore, the initial conditions and branch times were not specifically designed for this analysis. However, the spin-up experiment initialising on the 1st of August is suitable for analysing the WAM since this is the month over which the monsoon reaches its peak intensity.

2.3 Regions

Several regions are used in this analysis to capture different processes and mechanisms related to WAM precipitation change. Cross-sections of the atmosphere are calculated by taking a zonal mean between 10° W and 25° E, consistent with the bounds used by Shekhar and Boos (2017) (Fig. 4b green lines). In addition to these longitudinal bounds, the WAM region is characterised using GPCP observations between 1980 and 2010 and a box to approximate the region where the annual range in rainfall (June–August precipitation minus December–February precipitation) exceeds 180 mm and where the summer rainfall accounts for over 35% of the total annual rainfall (Wang and Ding 2006). Averages are taken over this WAM region, which extends from 10° W to 25° E and 7 to 15°

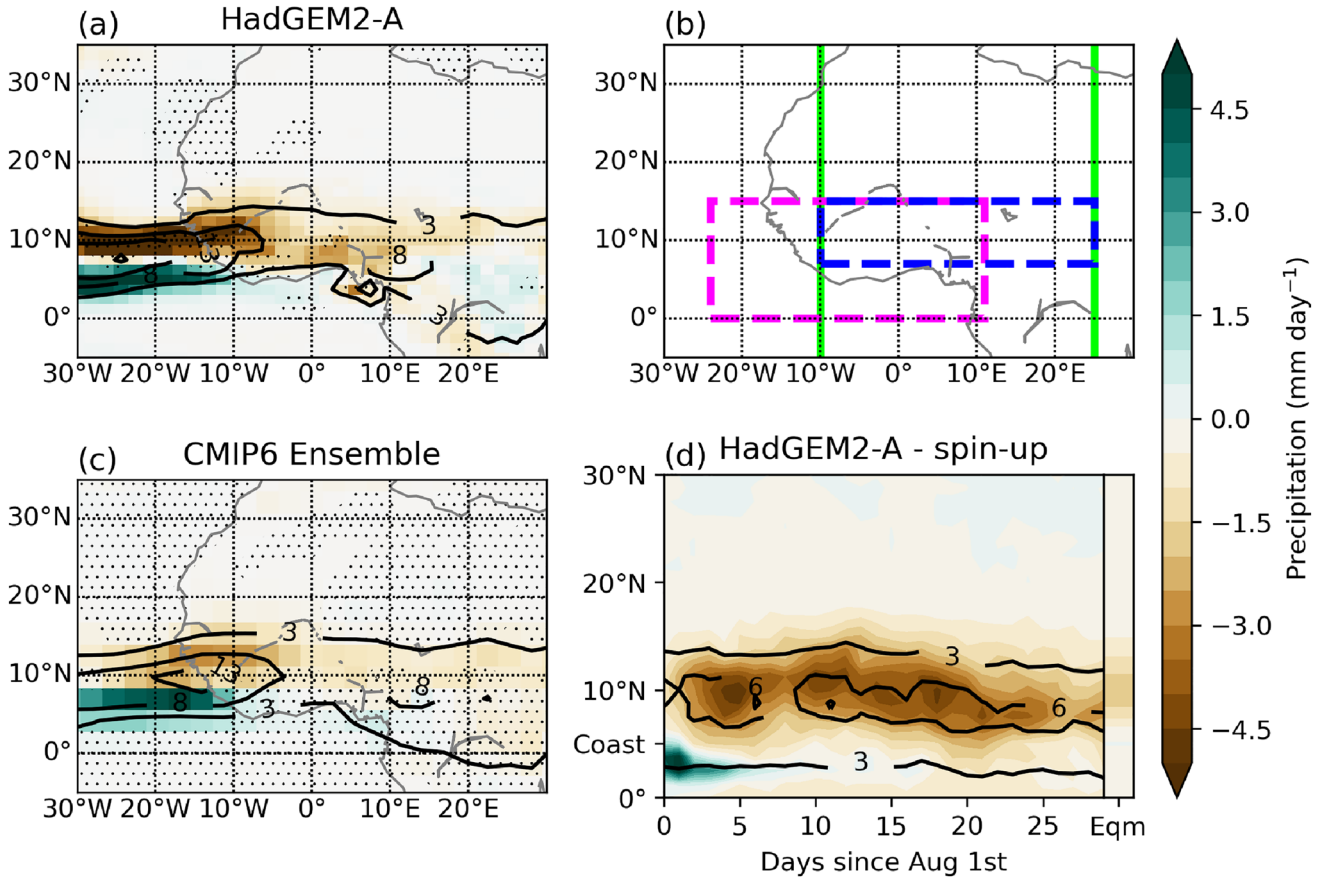

Fig. 4 **a** HadGEM2-A, and **c** 8 CMIP6 model ensemble mean, amip climatological (black lines) and amip-p4K - amip anomalous (colors) August precipitation. **a** Regions where anomalous HadGEM2-A precipitation lies outside the CMIP6 range are highlighted with stippling. **c** CMIP6 model agreement is highlighted using a t-test where the p value represents the probability of the ensemble mean being consistent with zero. Stippling represents regions with a p value greater than 0.05. **b** Regions used for analysis; green lines indicate the longitudinal bounds used for cross-section analysis, dashed blue box indicates West African monsoon region, and dashed magenta box indicates the region used to characterise the land vs ocean equilibrium precipitation responses in Fig. 18b. **d** (Left of vertical black line) HadGEM2-A spin-up experiment time–latitude plot of anomalous (amip-p4K-spinup - amip) precipitation, and (right of vertical black line) HadGEM2-A equilibrium anomalous (amip-p4K - amip) August precipitation. Here, for each day, precipitation has been zonally averaged between the green lines in **b**

N (Fig. 4b blue box). A third region is used to investigate the changes in the strength of the shallow meridional circulation over West Africa, again using the same longitudinal range and averaging meridionally between 8 -22° N (red lines in Fig. 9a). Finally, to investigate changes in land/ocean precipitation in the equilibrium experiment, a box covering 24° W–11° E and 0–15° N is used and a land mask is employed to characterise land and ocean precipitation (Fig. 4b magenta box). The ocean region in the magenta box in Fig. 4b is also used to characterise the changes in near surface specific humidity over the ocean in Sect. 3.2.

2.4 Definition of key quantities

A set of equations used to calculate equivalent potential temperature, Low Level Atmospheric Thickness (LLAT) (used to document changes in the shallow circulation), horizontal divergence of moisture transport, and other key quantities used in the analysis are presented in Appendix 2.

3 Results

WAM precipitation decreases in response to a uniform ocean warming both in the equilibrium response (Fig. 4a, c) and in the spin-up response (Fig. 4d). This equilibrium response is consistent with previous results of Gaetani et al. (2017); Held et al. (2005); Hill et al. (2017), however, the spin-up response has not previously been investigated. Here, the spin-up response highlights the time evolution from the day after the abrupt ocean warming towards the equilibrium state. Focusing on the equilibrium response (Fig. 4a, c), climatologically the monsoon rainband is seen around 10° N, with more precipitation over ocean compared to land. In response to a uniform SST increase, rainfall decreases across the whole monsoon region, with a weaker response towards the east. Over the ocean, the anomalous precipitation indicates both a slight decrease and a southward shift in the rainband. Comparing Fig. 4a and c, the precipitation response seen in HadGEM2-A is consistent with the CMIP6 ensemble mean. The CMIP6 ensemble mean demonstrates both a less intense climatological rainband and a weaker response to the warmer SSTs. The stippling in Fig. 4a highlights areas where the precipitation anomalies in HadGEM2-A are outside the range of precipitation anomalies seen in the CMIP6 ensemble. This shows that, for most regions, the HadGEM2-A response sits within the CMIP6 range. The regions where this is not the case are mainly over the West coast where the North–South dipole in precipitation change in the CMIP6 models is located further north compared to HadGEM2-A.

3.1 Spin-up Day 1

In order to understand how the equilibrium response is reached, the spin-up experiment is used to analyse the response over the first month following the uniform ocean warming. It is found that, after just one day of the spin-up experiment simulation, the WAM precipitation decreases. A moisture budget analysis of the first day of the spin-up experiment shows the anomalous precipitation, evaporation, moisture convergence and total column moisture (Fig. 5). The moisture budget stipulates that any changes in total column moisture are balanced by evaporation and moisture convergence into the column, and precipitation out of the column (Eq. 2) (Brown and Kummerow 2014; Trenberth et al. 2011). A large increase in precipitation over the ocean is seen, whilst inland, the precipitation decreases slightly. Due to the warmer SSTs, the evaporation and total column moisture increases over the ocean and remains largely unchanged inland. The moisture convergence map indicates enhanced convergence in regions where the precipitation increases, and reduced levels of convergence over land regions and over non-convective ocean regions. The moisture budget analysis in Fig. 5 indicates that the reduced WAM precipitation on day 1 of the spin-up experiment is primarily caused by a reduction in moisture convergence over the region.

To explore this decrease in moisture convergence and precipitation in the WAM region further, the anomalous 500 hPa temperature is shown in Fig. 6. Here, it is seen that the atmosphere over the ocean warms and this warming spreads inland over West Africa. This response occurs through boundary layer warming (due to warmer oceans) being efficiently transported upwards in the atmosphere through convection and, since large free tropospheric temperature gradients cannot be sustained at low latitudes, this warming is horizontally transported away efficiently through atmospheric waves to dissipate the pressure gradient that forms as a result of the temperature change. These processes can be explained through convective quasi-equilibrium and the Weak Temperature Gradient (WTG) approximation. Convective quasi-equilibrium suggests that, since convection occurs rapidly, the temperature profile of an atmospheric column tends towards a moist adiabatic lapse rate in regions of active deep convection. This means that in such regions, the temperature of the free troposphere is to some degree set by the moist static energy in the boundary layer (Emanuel et al. 1994). The WTG approximation postulates that at low latitudes, large free tropospheric temperature gradients cannot be sustained due to the small Coriolis parameter (Sobel et al. 2001). In Fig. 6, it is seen that the free tropospheric warming over the ocean spreads inland to maintain a weaker temperature gradient. This propagation of temperature away from the convective ocean regions warms the atmosphere inland, thus stabilising the atmosphere in the WAM region,

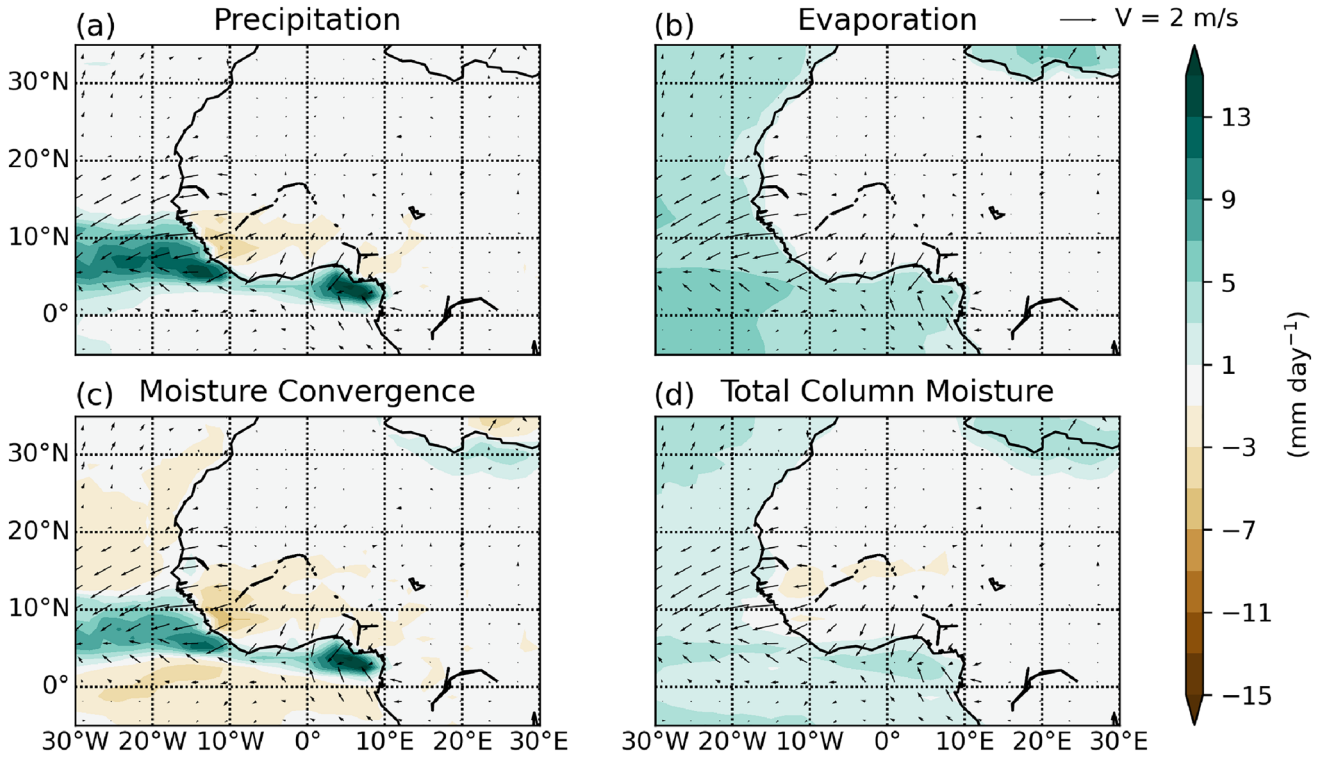

Fig. 5 HadGEM2-A spin-up experiment day 1 moisture budget analysis showing anomalous (amip-p4K-spinup - amip); **a** precipitation, **b** evaporation, **c** moisture convergence, and **d** total column moisture. spin-up experiment day 1 anomalous (amip-p4K-spinup - amip) 925 hPa winds are also indicated using arrows in **a–d**

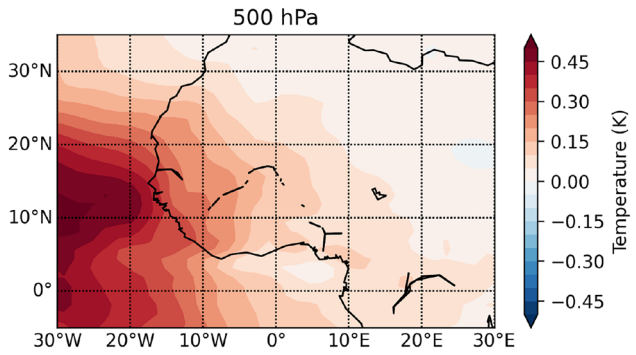

Fig. 6 HadGEM2-A spin-up experiment day 1 anomalous (amip-p4K-spinup - amip) 500 hPa temperature

acting to inhibit convection (Caminade and Terray 2010; Herceg et al. 2007).

To demonstrate that this advection of temperature inland stabilises the atmosphere in the monsoon region on the first day of the spin-up experiment, vertical profiles of equivalent potential temperature (θ_e) and saturation equivalent potential temperature (θ_{es}) over the WAM region are shown in Fig. 7 (calculated using Eq. 3 (Stull 1988)), with the anomalies presented in Fig. 7a, and the climatology shown in 7b. Since the increase in free tropospheric (roughly 700–300 hPa) θ_{es}

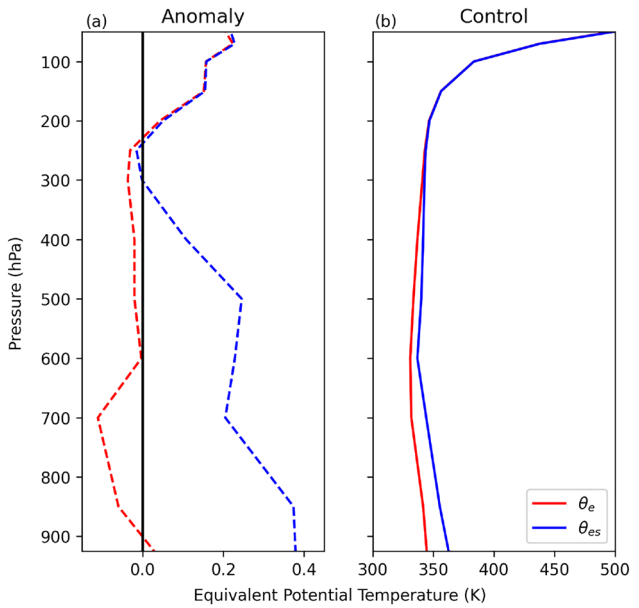

Fig. 7 HadGEM2-A spin-up experiment day 1; **a** anomalous (amip-p4K-spinup - amip), and **b** control (amip), equivalent potential temperature θ_e (red) and saturation equivalent potential temperature θ_{es} (blue) averaged over the WAM region (10° W–25° E and 7–15° N)

exceeds the changes in boundary layer θ_e, the atmosphere is more stable (in a moist sense, i.e. considering θ_e not just θ) on the first day of the spin-up experiment. This increase in stability over the WAM region is consistent with the decrease in precipitation in Fig. 5a.

The WAM precipitation is also influenced by disruptions to the monsoon inflow at low levels. The warmer SSTs on the first day of the spin-up experiment warms the atmosphere over the ocean more than over the land (Fig. 8a). This differential warming occurs in the boundary layer due to the abrupt ocean warming and the lack of changes to land surface temperatures. A map indicating the percentage of atmospheric warming over the ocean occurring in the lower levels of the atmosphere (1000–700 hPa) shows that over 50% of the warming occurs in the lowest 300 hPa (Fig. 8b). This atmospheric warming causes differential changes to surface pressure patterns, with lower pressures over the ocean compared to the land (Fig. 8a). These surface pressure changes generate an anomalous wind at low levels from land to ocean, opposing the climatological monsoon flow. This weakening of the monsoon inflow at low levels reduces the convergence of moisture inland and leads to a reduction in precipitation. This reduced level of moisture convergence inland is consistent with the results presented in Fig. 5.

To summarise, on day 1 of the spin-up experiment, precipitation is reduced through enhanced convection over the ocean, stabilising the atmosphere inland, and through temperature and pressure changes that cause reduced levels of moisture convergence at the surface in the monsoon region.

3.2 Spin-up transition towards equilibrium response

As discussed in Sect. 3.1, the immediate WAM response to an abrupt SST warming is for the precipitation to decrease. Here, the remainder of the spin-up experiment is analysed and compared to the equilibrium response, to show how different mechanisms affect the WAM on different timescales, and how these mechanisms relate to the long term WAM precipitation response.

Figure 4d shows a time-latitude plot of precipitation, zonally averaged from 10° W–25° E. The initial increase in precipitation over the ocean persists for the first few days of the spin-up experiment but becomes much weaker after day 7. In contrast, the decrease in precipitation over the WAM region is evident throughout the spin-up experiment and into the equilibrium response. It is likely that the decrease in precipitation is largely caused by dynamical changes to the WAM circulation or through more subtle effects of changes in moisture and moisture gradients (Chadwick et al. 2016). The large-scale moistening of the atmosphere will also likely have an impact on WAM precipitation (i.e. a thermodynamically driven increase in rainfall). However, this effect is evidently not dominating the response since the precipitation decreases.

Climatologically, two key circulations are associated with the WAM; a deep circulation, ascending through the depth of the troposphere at about 10° N, and a shallow circulation, ascending to around 700 hPa and extending further northwards to 15° N (Fig. 3) (Mutton et al. 2022; Gaetani et al. 2017; Zhang et al. 2008). The deep circulation is associated with the Hadley cell, with the ascending branch being closely linked to the monsoon rainband. The shallow circulation is a thermally direct circulation closely linked to the Saharan heat low. Climatologically, this shallow circulation tends to advect dry air into the monsoon rainband at mid-levels, acting to inhibit WAM precipitation. Shekhar and Boos (2017) demonstrated that the strength and meridional extent of the shallow circulation is associated with changes in WAM precipitation. As indicated in Fig. 3, a strong and southward shifted shallow circulation is associated with a drier WAM.

To investigate how this shallow circulation responds to a uniform SST warming, plots of 700 hPa horizontal moisture

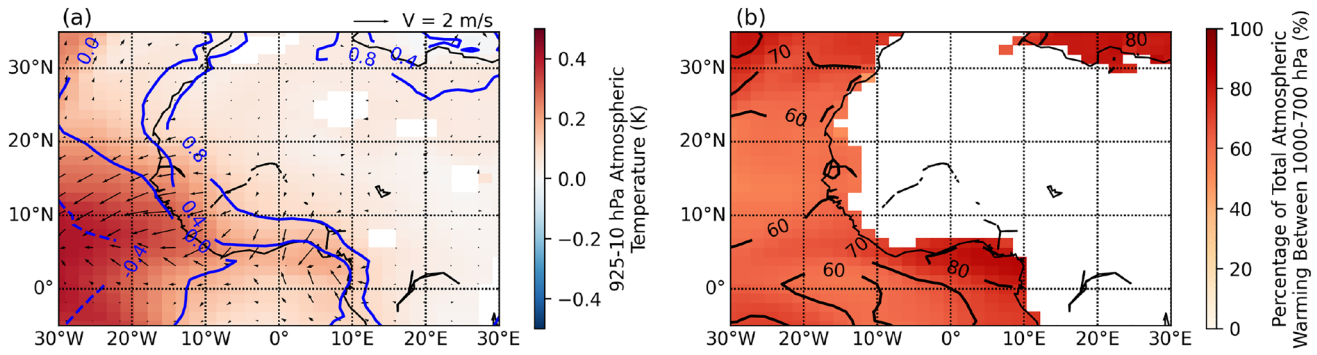

Fig. 8 HadGEM2-A spin-up experiment day 1; **a** anomalous (amip-p4K-spinup - amip); mass weighted column mean temperature (colors), sea level pressure (blue lines), and 925 hPa winds (arrows), and **b** percentage of mass weighted column mean temperature change occurring between 1000 and 600 hPa. Black lines indicate 60, 70, and 80% contours. Grid boxes masked by orography are shown in white

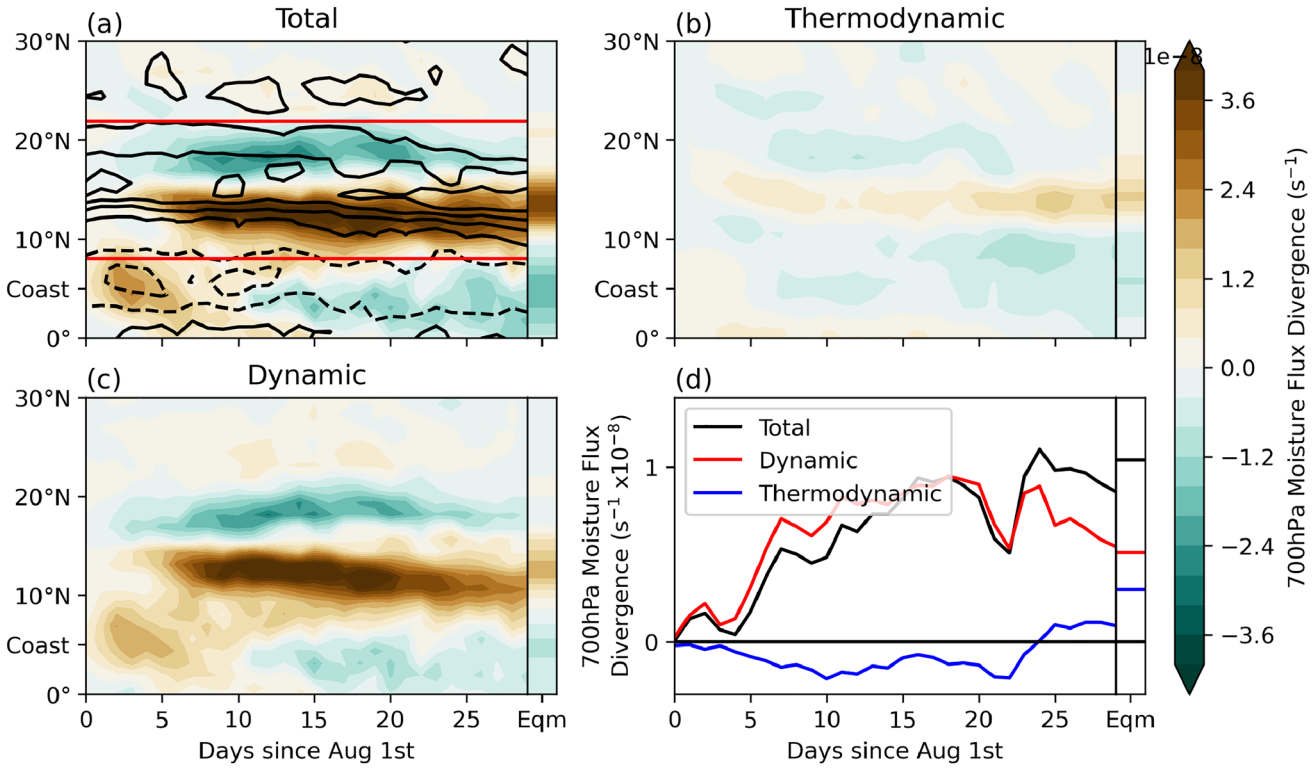

Fig. 9 HadGEM2-A (**a**) (left of vertical black line) climatological (amip) (black lines) and spin-up anomalous (amip-p4K-spinup - amip) (colors) 700 hPa horizontal moisture flux divergence. Red lines indicate the region used to average meridionally to produce Fig. 9d. (right of vertical black line) equilibrium anomalous (amip-p4K - amip) August 700 hPa horizontal moisture flux divergence. **b** Thermodynamic, and **c** Dynamic component of (left of vertical black line) spin-up anomalous (amip-p4K-spinup - amip) 700 hPa horizontal moisture flux divergence, and (right of vertical black line) equilibrium anomalous (amip-p4K - amip) August 700 hPa horizontal moisture flux divergence. **d** HadGEM2-A (left of vertical black line) spin-up anomalous (amip-p4K-spinup - amip), and (right of vertical black line) August equilibrium anomalous (amip-p4K - amip); horizontal moisture flux divergence (black), dynamical component of anomalous 700 hPa horizontal moisture flux divergence (red), and thermodynamic component of anomalous 700 hPa horizontal moisture flux divergence (blue), averaged between 8 and 22° N. Zonal averages taken between 10° W and 25° E

flux divergence are shown in Fig. 9. A time-latitude plot of 700 hPa moisture divergence is presented in Fig. 9a, and a decomposition of the change in moisture flux divergence into thermodynamic and dynamic terms is shown in Fig. 9b and c respectively (Eqs. 6 and 7). Figure 9d highlights the change in strength of 700 hPa moisture flux divergence associated with the shallow circulation by averaging the total, thermodynamic, and dynamic terms meridionally between 8 and 22° N (see horizontal red lines in Fig. 9a). These bounds are used to capture both positive and negative components of the dipole caused by the circulation shift, therefore isolating the change in strength of moisture flux divergence. Climatologically, a maximum in moisture flux divergence is seen around 15° N, associated with the outflow from the ascending branch of the shallow circulation (Fig. 9a black lines). By roughly day 5 of the spin-up experiment, this region of divergence strengthens (Fig. 9d black line) and shifts southwards (Fig. 9a colors), indicating a strengthening and a southward shift of the shallow circulation over West Africa. Decomposing this change in moisture flux divergence into a dynamic and a thermodynamic component, it is shown that the response in the spin-up experiment is largely dynamically driven, particularly for the first 20 days after the abrupt ocean warming (Fig. 9b–d). The thermodynamic component remains negligible for most of the spin-up experiment. However, after day 20, this component begins to play a more significant role in the total change in moisture flux divergence. The moisture flux divergence response in the equilibrium experiment can also be seen in Fig. 9 (panel right of vertical black line in each plot). Here, the strengthening of the moisture flux divergence persists, and the two thermodynamic and dynamic components both contribute to this strengthening, with the dynamic component slightly larger than the thermodynamic component (Fig. 9d). Calculating the change in strength of moisture flux divergence in the equilibrium experiment as a percentage, a 94% increase is seen. This strengthened moisture flux divergence at 700 hPa inhibits WAM precipitation through the advection of dry air into the monsoon rainband, contributing to the reduction in precipitation seen in the spin-up and equilibrium experiments.

Here, horizontal moisture flux divergence has been used to describe how changes relating to the shallow circulation can impact the WAM. Changes in this moisture flux divergence have been decomposed into dynamic and thermodynamic terms to highlight the relative contributions from changes in circulation or moisture and moisture gradients respectively. However, in order to fully highlight how the circulation itself changes relative to the climatological circulation, climatological and anomalous horizontal divergence of winds have been shown in Fig. 10a, and climatological and anomalous zonal winds have been shown in Fig. 10b. Climatologically the mid-level divergence associated with the shallow circulation can be seen at 15° N and 700 hPa. In response to the uniform SST warming, this region of divergence strengthens and shifts southwards (consistent with the results shown in Fig. 9). The divergence at 7° N and 200 hPa associated with the monsoon rainband is shown to weaken, consistent with reduced convection and precipitation. The zonal winds in Fig. 10b also capture important changes in the circulation. The strong climatological easterlies seen at 10° N and 700 hPa highlight the location of the African easterly jet. The African easterly jet influences WAM precipitation through its role in the formation of mesoscale convective systems (Besson and Lemaitre 2014), and through its influence on the large scale circulation (Cook 1999). The former of which is not simulated realistically in GCMs due to their coarse resolution. On the impact of the African easterly jet on the large scale circulation, Cook (1999) suggests that the presence of the jet inhibits moisture convergence. This is consistent with the results of Figs. 9 and 10b, where both the location of horizontal moisture flux divergence and the African easterly jet are shifted southwards.

Since the shallow meridional circulation is closely linked to the Saharan heat low, changes in temperature and LLAT over West Africa can influence changes in the circulation. LLAT is defined as the difference in geopotential heights between 700 and 925 hPa (Eq. 8) and can be used to monitor changes in the Saharan heat low (Lavaysse et al. 2009). Time-latitude plots of LLAT, meridional gradient of LLAT, and meridional winds at 925 hPa are shown in Fig. 11.

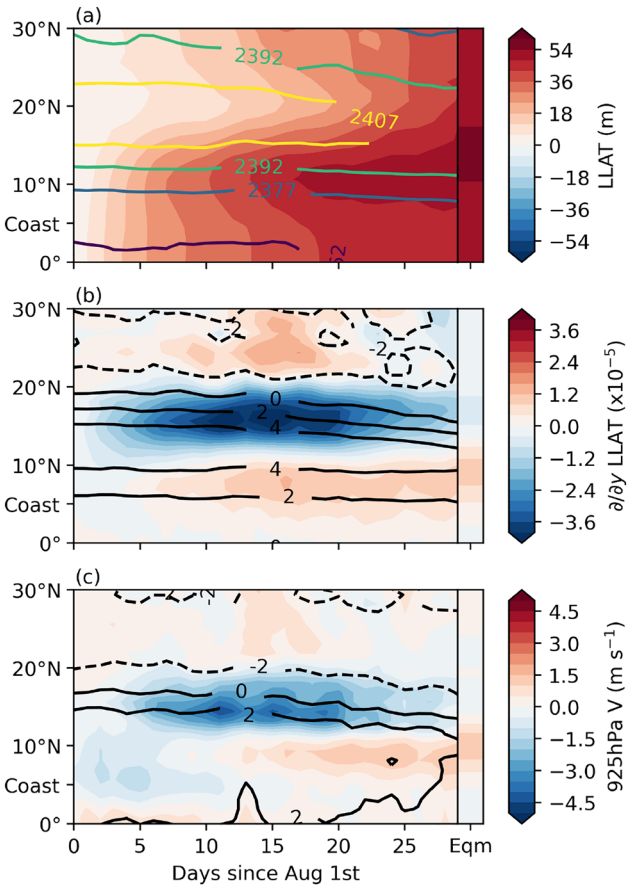

Fig. 11 HadGEM2-A (left of vertical black line) climatological (amip) (lines), and spin-up anomalous (amip-p4K-spinup - amip) (shaded colors), and (right of vertical black line) August equilibrium anomalous (amip-p4K - amip); **a** LLAT, **b** meridional LLAT gradient, and **c** 925 hPa meridional winds

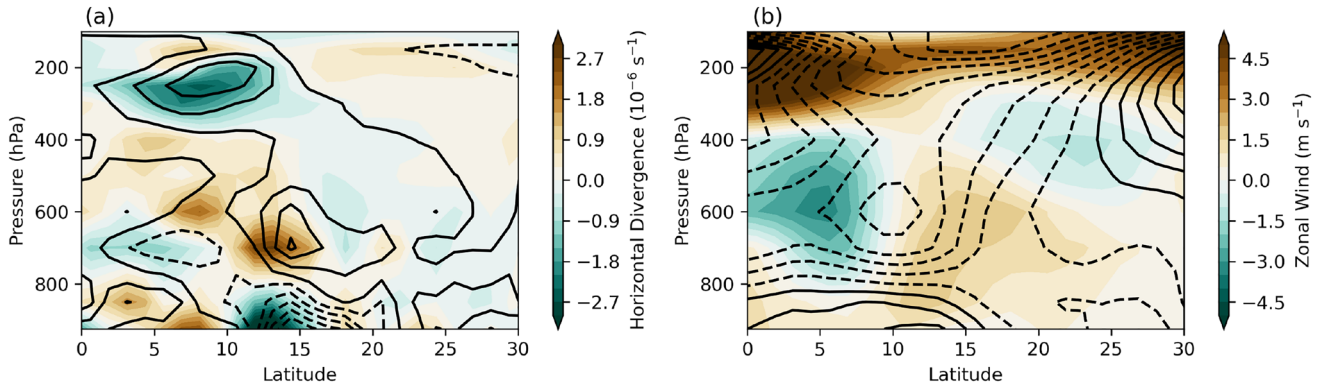

Fig. 10 HadGEM2-A August **a** zonally averaged horizontal divergence of winds and **b** zonally averaged zonal winds. Climatological (amip) values indicated with lines and anomalies (amip-p4K - amip) in colors. Zonal averages taken between 10° W and 25° E

Here, the climatological values are shown with lines and the anomalies are indicated by the shaded colors. The spin-up results are presented to the left of the vertical black line and the equilibrium response shown to the right. The initial response, seen over the first 5 days of the spin-up experiment, is for the atmosphere to warm more over the ocean (and in the ocean sourced monsoon airmass) compared to the dry desert region further inland. This is seen in Fig. 11a where the LLAT increase is larger to the south of 15° N. The LLAT changes generate a large-scale meridional gradient in LLAT (Fig. 11b), and the meridional winds respond accordingly with a southward anomaly. The change in meridional winds shown in Fig. 11c is consistent with a southward shift in the shallow circulation, a response seen in the 700 hPa moisture flux divergence shown in Fig. 9.

After roughly day 7 of the spin-up experiment, a warm tongue between 10–15° N begins to form. This causes a positive LLAT gradient anomaly to the south and a negative LLAT gradient anomaly to the north of the maximum in anomalous LLAT. Again, the meridional winds respond to these gradient changes, and a northward wind anomaly is seen to the south of the LLAT maximum and a southward wind anomaly is seen to the north. These changes in low level wind are consistent with a strengthening and southward shift of the low level convergence associated with the shallow circulation (as seen in Fig. 9).

By day 20 of the spin-up experiment, the warming to the north of 15° N has begun to catch up with the warming to the south, and the large-scale LLAT gradient anomalies begin to weaken, reflected in a weakening of the southward meridional wind anomaly after day 20. By the equilibrium experiment (Fig. 11 right of the vertical black line), the large-scale gradient in temperature between the ocean and the dry desert airmass is no longer apparent. The warm tongue between 10 and 15° N persist however, generating a positive LLAT gradient anomaly to the south and negative LLAT gradient anomaly to the north. The meridional winds respond accordingly with a southerly wind anomaly to the south of the LLAT maximum and an (albeit small) northerly wind anomaly to the north, again consistent with a strengthening of the shallow meridional circulation seen in the equilibrium response presented in Fig. 9.

The maximum increase in LLAT seen in Fig. 11a is located over the Southern Sahel (between 10 and 15° N). The Sahel is a semi-arid region where the sparse vegetation cover means that surface heat fluxes are strongly controlled by the amount of precipitation falling over the previous days. This is not the case for the regions to the south with denser vegetation cover since the plant roots are able to access moisture from deeper underground (Lohou et al. 2014). In the Sahel, a reduced level of precipitation leads to a reduction in surface latent heat flux. This reduced latent heat flux is largely balanced by an increase in sensible heat

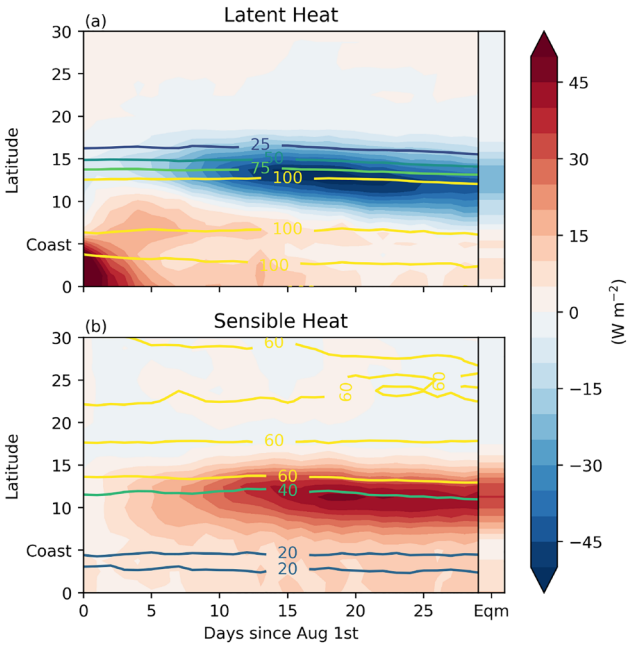

Fig. 12 HadGEM2-A (left of vertical black line) climatological (amip) (lines) and spin-up anomalous (amip-p4K-spinup - amip) (shaded colors) and (right of vertical black line) August equilibrium anomalous (amip-p4K - amip); **a** latent heat flux, and **b** sensible heat flux

flux, which in turn warms the atmosphere above the surface. To demonstrate this, time latitude plots of surface latent and sensible heat are shown in Fig. 12. Over the first 5 days of the spin-up experiment, the warmer oceans lead to a large increase in latent heat flux south of 5° N. Inland, the decrease in precipitation over the Sahel is associated with a decrease in latent heat flux and an increase in sensible heat flux, with the strongest response seen between 10 and 15° N. This is the region over which the precipitation anomaly is sufficiently negative (Fig. 4d) and the surface is more water-limited (i.e. where the latent heat flux is largely controlled by the amount of precipitation that falls over the previous days). These changes in sensible heat flux warm the atmosphere and form the warm tongue seen in the LLAT response in Fig. 11a. This surface heat flux response to a decrease in precipitation can act as a positive feedback mechanism, with the increase in LLAT generated by the sensible heat flux anomalies over the Sahel causing changes in circulation that then lead to further reductions in precipitation. This mechanism could help sustain the strengthening of the shallow circulation, even when the large scale LLAT gradient of a warmer ocean and cooler land no longer persists.

To help further demonstrate the relationship between the soil moisture feedback and changes in circulation, the latent heat flux, sensible heat flux, and 925 hPa wind anomalies between the amip-p4K and amip experiments have been plotted in Fig. 13. The regions with decreased latent heat

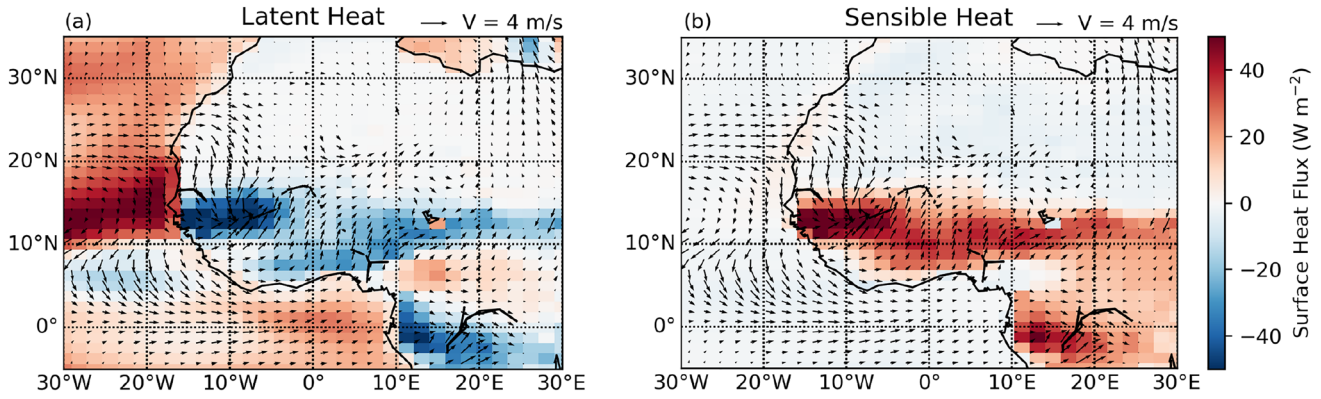

Fig. 13 HadGEM2-A anomalous (amip-p4K - amip) August **a** latent heat flux and **b** sensible heat flux (colors) and **a**, **b** 925 hPa winds (arrows)

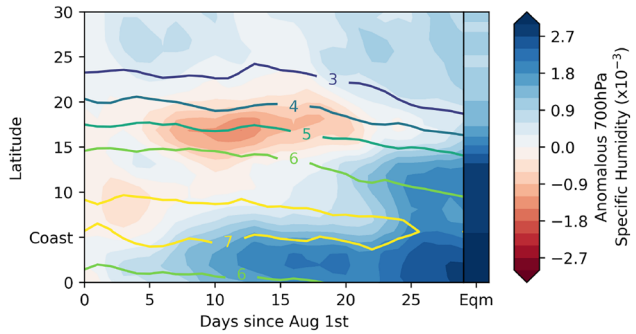

Fig. 14 HadGEM2-A (left of vertical black line) climatological (amip) (lines) and spin-up anomalous (amip-p4K-spinup - amip) and (right of vertical black line) August equilibrium anomalous (amip-p4K - amip) 700 hPa specific humidity

flux also have an increased sensible heat flux. These regions exhibit the larger wind anomalies, helping to show how the surface heat flux response to the reduction in precipitation leads to a change in circulation.

So far, the dynamic response to an abrupt ocean warming has been investigated, showing how the combined effects of differential warming between land and ocean and a soil moisture feedback mechanism can lead to a southward shift and strengthening of the shallow circulation and a decrease in WAM precipitation. However, towards the end of the spin-up experiment and into the equilibrium response, the thermodynamic changes associated with the shallow circulation become more significant and play a larger role in strengthening the dry air advection into the monsoon rainband in the lower free-troposphere (Fig. 9b).

To investigate these thermodynamic changes, a time–latitude plot of 700 hPa specific humidity is shown in Fig. 14. Over the first 10 days of the spin-up run, the specific humidity gradually increases over the ocean (south of 5° N) and decreases slightly inland. After day 5, north of 15° N, the specific humidity decreases likely associated with a southward shift in the boundary between the dry desert airmass and the moist monsoon airmass. After day 20 of the spin-up run, the specific humidity increases inland, a response mostly located south of 15° N, as this is the approximate boundary of the low-level monsoon airmass. Further north, the increase in specific humidity is weaker. This differential change in specific humidity leads to a strengthened meridional gradient in specific humidity, thus leading to a thermodynamic increase in the efficiency of which southerly dry air advection dries out the monsoon rainband at 700 hPa (Fig. 9b). In the equilibrium experiment, this response is even clearer, with an even stronger gradient in specific humidity anomalies between 10 and 15° N, again, consistent with the increase in the thermodynamic component of the 700 hPa moisture flux divergence anomalies in the equilibrium experiment shown in Fig. 9b, d. This mechanism whereby enhanced moisture gradients in the lower free-troposphere inhibits WAM precipitation is consistent with the findings of Hill et al. (2017). There, a moist static energy budget analysis was used to investigate the Sahel precipitation response to a uniform ocean warming. It was found that enhanced moist static energy gradients in the mid-troposphere strengthened the advection of low moist static energy into the monsoon rainband. This increase in low moist static energy advection was balanced by a decrease in vertical motion in the rainband, thus inhibiting precipitation.

This specific humidity response to a uniform ocean warming, whereby the moist regions get more moist relative to the dryer regions, is consistent with the work of Chadwick et al. (2016) and Byrne and O'Gorman (2016). They suggest that changes in specific humidity over land in response to SST warming could be determined by scaling the present day specific humidity by the fractional increase in the near surface specific humidity over the ocean. To investigate this in the equilibrium response presented in Fig. 14, a scatter plot of control (amip) against anomalous (amip-p4K - amip) 700 hPa specific humidity across the latitudes

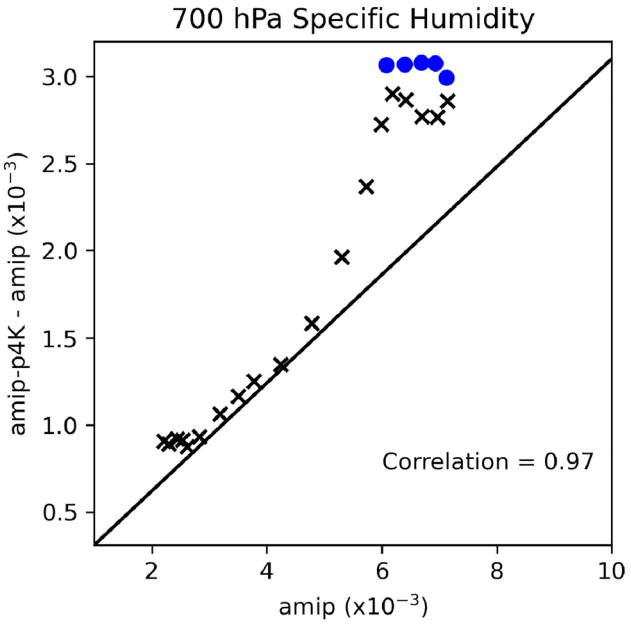

Fig. 15 Scatter plot of control (amip) against anomalous (amip-p4K - amip) 700 hPa specific humidity at each latitude point between 0 and 30° N averaged across the green cross section area indicated in Fig. 4b. Blue circles indicate ocean regions and black crosses indicate land regions. The diagonal black line indicates the specific humidity scaling based on the percentage change in 1000 hPa specific humidity over the ocean in the magenta box in Fig. 4b between amip and amip-p4K experiments (31%)

presented in Fig. 14 is shown in Fig. 15. The diagonal black line across the axis highlights the fractional change in near surface (1000 hPa) specific humidity over the ocean in the magenta box in Fig. 4b, where a 31% increase in specific humidity is calculated. This 31% increase in near surface specific humidity is consistent with what might be expected if specific humidity were to increase in line with atmospheric temperatures under the Clausius–Clapeyron equation (assuming no changes in relative humidity). Under this equation an approximate 7% K^{-1} increase in specific humidity would be expected (Held and Soden 2006). Therefore, with a warming of 4K, this Clausius–Clapeyron scaling predicts a 28% increase in near surface specific humidity (assuming no dynamical changes). The scatter plot shown in Fig. 15 indicates that the changes in 700 hPa specific humidity over West Africa are largely consistent with the scaling of near surface ocean specific humidity, and the smaller deviations from this scaling are likely caused by dynamic changes in circulation such as the position of airmass boundaries or by changes in surface evaporation. It is important to note that the method presented by Chadwick et al. (2016) looked at changes in near surface specific humidity, whereas here, the scaling is applied to 700 hPa specific humidity. Despite this, the scaling still appears to hold reasonably well, with some larger deviations in the more moist regions.

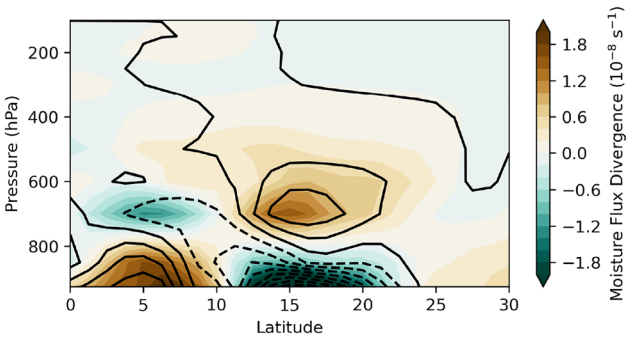

Fig. 16 Zonally averaged June–August horizontal moisture flux divergence climatology (lines), and amip-p4K - amip anomaly (colors) in the CMIP6 ensemble mean. Zonal averages taken between 10° W and 25° E

3.3 Equilibrium response

Section 3.2 investigated the response to an abrupt uniform ocean warming over the first month following the SST increase. The analysis examines the mechanisms that can influence precipitation and suggests how the response moves through the spin-up time frame towards the equilibrium response. This section aims firstly to demonstrate that the mechanisms identified in HadGEM2-A are also present in the CMIP6 ensemble equilibrium response, and secondly, to investigate whether there is evidence to show that the mechanisms identified in the spin-up experiment also apply during the seasonal cycle of the equilibrium response.

One mechanism identified in Sect. 3.2 involves changes in the shallow meridional circulation over West Africa. It was shown that both dynamically, through a strengthening of the circulation, and thermodynamically, through enhanced moisture gradients over the Sahel, enhanced horizontal moisture flux divergence at 700 hPa is associated with a decrease in WAM precipitation (consistent with Shekhar and Boos (2017)). A cross-section of horizontal moisture flux divergence in the CMIP6 model ensemble mean, zonally averaged between 10° W and 25° E, is shown in Fig. 16. Consistent with the response seen in HadGEM2-A, the CMIP6 ensemble mean also exhibits a strengthening of the horizontal moisture flux divergence associated with the shallow circulation.

In Sect. 3.2, the cause of this enhanced moisture flux divergence at 700 hPa was also investigated. Firstly, the combined impact of changing LLAT gradients and a soil moisture feedback influenced changes in circulation. Figure 17 shows that the response seen in HadGEM2-A is consistent with that seen in the CMIP6 ensemble mean. Figure 17a highlights the decrease in precipitation over the WAM region in response to ocean warming and Fig. 17b shows the surface heat flux response. Over the Sahel, the decreased precipitation is associated with a decrease in

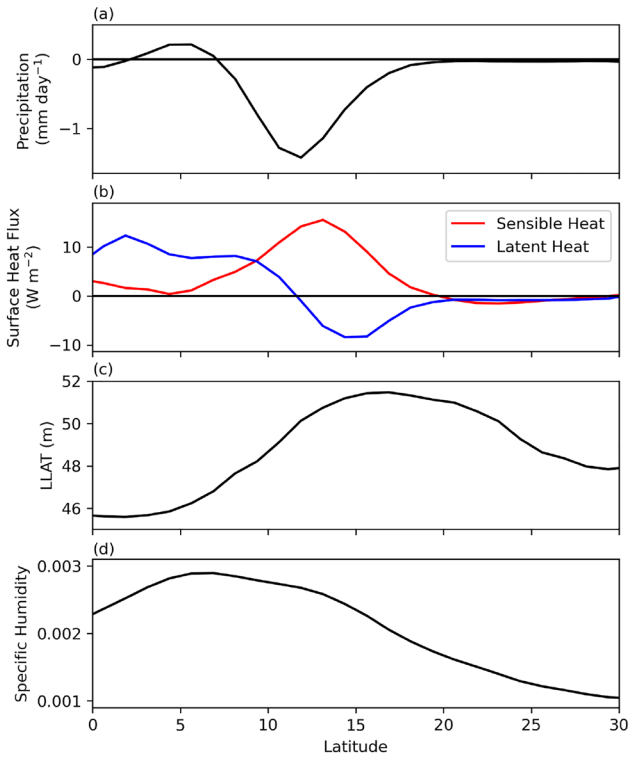

Fig. 17 Zonally averaged June–August amip-p4K - amip anomalous **a** precipitation, **b** surface heat fluxes, **c** LLAT, and **d** 700 hPa specific humidity in the CMIP6 ensemble mean. Zonal averages taken between 10° W and 25° E

latent heat flux and an increase in sensible heat flux. These sensible heat flux anomalies influence temperature changes over West Africa and a maximum in anomalous LLAT can be seen over the Sahel (Fig. 17c). The second way in which the enhanced moisture flux divergence at 700 hPa is explained in Sect. 3.2 is through enhanced gradients in specific humidity between the moist monsoon airmass and the drier desert airmass. More moistening was seen in the climatologically moist regions compared to the climatologically dry regions. Again, Fig. 17d shows that the response seen in HadGEM2-A is consistent with the CMIP6 ensemble mean. The 700 hPa specific humidity increase is greater to the South compared to the North. This specific humidity gradient over the Sahel can increase the efficiency at which southerly dry air advection dries out the monsoon rainband at 700 hPa.

Thus far in this section we have shown that the mechanisms involving changes in the shallow circulation, a soil moisture feedback and an increased gradients in specific humidity are not only found in the HadGEM2-A spin-up analysis but are also seen in the CMIP6 ensemble mean equilibrium response. However, in Sect. 3.1 it was shown that over the first 5 days of the spin-up response, WAM precipitation decreases due to the stabilising affect of increased convective heating over the ocean and due to enhanced boundary layer warming over the ocean affecting the monsoon inflow at low levels through changing pressure gradients. In the spin-up experiments we have seen that this mechanism holds for the transient adjustment to ocean warming but it is unclear whether the mechanism also holds as we move towards equilibrium. Here, we investigate the possibility that this mechanism identified in the spin-up experiment could apply to the the seasonal cycle of the equilibrium response.

The seasonal cycle of the equilibrium response to a uniform ocean warming, as well as the climatological seasonal cycle is shown in Fig. 18. Here, the average over all years and every model has been calculated. All models shown in Fig. 1 have been used minus CNRM-CM6-1 due to data availability. In Fig. 18a a time-latitude plot of anomalous LLAT is shown (colors) and the climatological LLAT (lines) highlights the seasonal formation of the

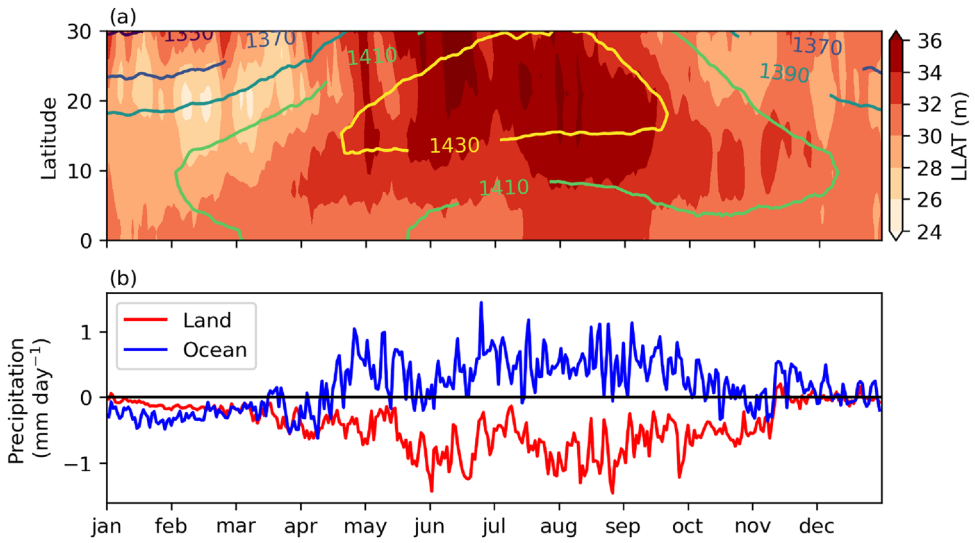

Fig. 18 7 CMIP6 model ensemble mean of seasonal **a** LLAT amip climatology (lines) and amip-p4K - amip anomaly (colors), and **b** changes in amip-p4K - amip anomalous mean land/ocean precipitation. Land and ocean precipitation averaged over the land/ocean regions within the magenta box in Fig. 4b

Saharan heat low which reaches its peak over the summer months. The LLAT anomalies prior to the main monsoon season are larger south of 10° N (over the ocean and ocean sourced monsoon airmass) compared to the desert regions to the north (although some larger values north of 25° N are also seen). This exhibits similar anomalous LLAT patterns to those seen in the first 5 days of the spin-up experiment (Fig. 11a). Alongside this, Fig. 18b shows that between May and October, positive precipitation anomalies are present over the ocean, again, similar to the response seen over the first 5 days of the spin-up experiment. These two results suggest that the WAM precipitation may be reduced in the equilibrium response due to differential warming over the land and ocean and enhanced oceanic precipitation, consistent with the response seen in the early stages of the spin-up experiment. Here we are suggesting it is possible that processes that manifest during the initial adjustment to SST warming may also be important at the start of each monsoon season during the equilibrium response. At the start of the spin-up experiment, the enhanced warming over the ocean compared to inland is most likely caused by the initial forcing being based over the ocean and the land warming taking time to adjust to this forcing. However, in Fig. 18a the warmer ocean–cooler land seen between January and May (i.e. the run up to the monsoon season) is likely caused by different processes. Despite this, the impact of this warming pattern on monsoon precipitation may still be similar.

The results shown in this section suggest that the mechanisms identified in the HadGEM2-A spin-up experiment are not only relevant when considering the transition towards the long term response, but are also useful for understanding how this response is sustained once the steady state equilibrium response has been reached.

4 Summary of results

This paper investigates the mechanisms behind a decrease in WAM precipitation in response to a uniform ocean warming. It is suggested that the decrease in precipitation is largely caused by dynamical changes to the WAM circulation or through more subtle effects of changes in moisture and moisture gradients (Chadwick et al. 2016). Consistent with the results of Monerie et al. (2020), the thermodynamically driven increase in rainfall associated with the large-scale moistening of the atmosphere does not dominate the response. A set of spin-up experiments are used to analyse the response over the days following the abrupt ocean warming, finding the precipitation decrease is caused by several mechanisms acting over a range of timescales following the SST perturbation.

The first mechanism identified in the spin-up analysis is shown to act within the first day of the experiment. Enhanced warming over the ocean increases convection and precipitation over the ocean, causing the atmosphere to warm at mid-levels. This atmospheric warming spreads inland and acts to stabilise the atmosphere over the monsoon region (Fig. 19a). The enhanced atmospheric warming over the ocean (largely at lower levels) also acts to influence low level winds by generating an anomaly directed from land to ocean. This anomalous wind disrupts the monsoon inflow and reduces the amount of moisture convergence inland, thus reducing the moisture supplied to the monsoon rainband and reducing precipitation.

The second mechanism identified in the spin-up analysis suggests that a reduction in precipitation is caused by a strengthening of the shallow meridional circulation, which tends to advect dry air into the monsoon airmass at mid-levels. A strengthening of this circulation advects more dry air into the rainband and can inhibit precipitation (Fig. 19b).

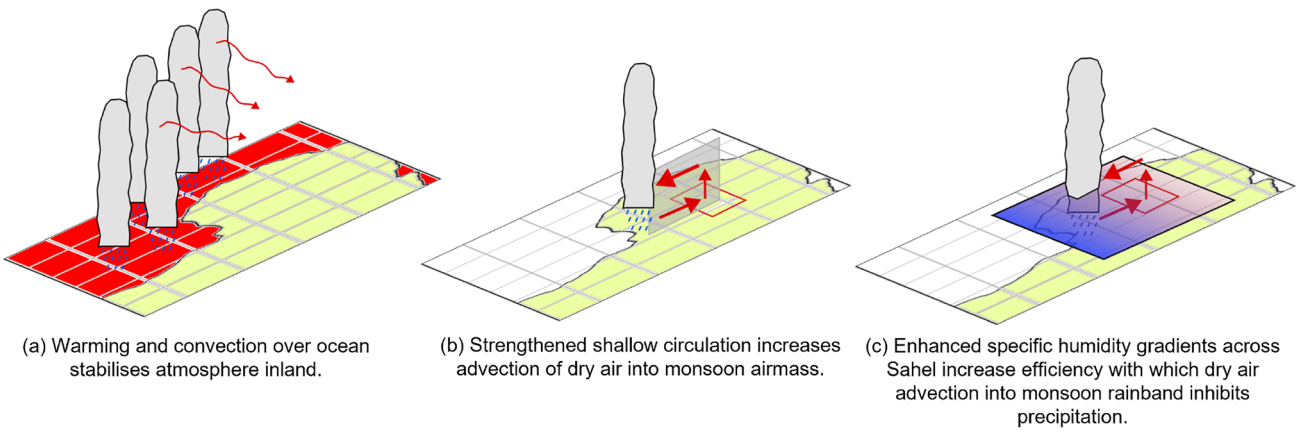

Fig. 19 Schematic depicting three key mechanisms that lead to a decrease in WAM precipitation in response to a uniform ocean warming

Since the shallow circulation over North Africa is thermally direct and closely linked to the Saharan heat low, changes in temperature and atmospheric thickness can affect the location and strength of the circulation. At the start of the spin-up run, the ocean warms more than the land, generating a large-scale meridional gradient in anomalous LLAT, with larger LLAT anomalies to the south and smaller anomalies to the north. This large-scale gradient causes the shallow circulation to shift southwards and strengthen, inhibiting precipitation in the WAM.

The third mechanism affecting the WAM precipitation involves a soil moisture feedback mechanism in the semi-arid Sahel region. In this region, due to the sparse vegetation cover, the surface heat fluxes are particularly sensitive to the precipitation that falls over the previous days. When less rain falls, the ground is dryer and there is less moisture available for evaporation. This reduced soil moisture causes a decrease in latent heat flux at the surface, which is approximately balanced by an increase in sensible heat flux. The increase in sensible heat flux warms the atmosphere over the Sahel and leads to a local LLAT maximum in the region. The local maximum in anomalous LLAT causes the shallow circulation over North Africa to strengthen and helps to sustain the circulation changes even when the large-scale meridional gradient in anomalous LLAT is no longer present.

The final mechanism identified through the spin-up analysis leading to a reduction in WAM precipitation involves an increased meridional gradient in specific humidity at 700hPa. In response to ocean warming, the moist monsoon airmass experiences a larger moistening compared to the dryer desert airmass, leading to a strong gradient in anomalous specific humidity between 10 and 15° N. This anomaly increases the efficiency at which dry air advection into the monsoon airmass at 700 hPa acts to inhibit precipitation (Fig. 19c).

Using an ensemble of CMIP6 models, it has been shown that each of the mechanisms identified in the spin-up experiment may also be present in the long term equilibrium response where the atmosphere has reached a steady state.

5 Discussion and conclusions

The WAM is depended on by a large population with relatively low adaptive capacity. Because of this, it is important that any adaptation strategies in the region are well informed by accurate climate projections. Currently, the uncertainty in WAM precipitation projections is large, and in order to address this, a greater understanding of the mechanisms and processes that influence the WAM in response to increased CO_2 should be obtained. By breaking down the full forcing of increased CO_2 into a number of direct and indirect effects it is possible to simplify the analysis and highlight different processes that influence precipitation in the WAM region. Here, the impact of a uniform ocean warming on the WAM has been investigated. In response to a uniform SST warming, the precipitation associated with the WAM is expected to decrease. Despite this being a consistent response seen across a range of CMIP5 and CMIP6 models and having been investigated in previous literature, the mechanisms behind this decrease in precipitation are yet to be fully understood.

The results highlight several mechanisms that act to cause a decrease in WAM precipitation in response to a uniform ocean warming. These results, alongside the results from a companion paper examining the response of the WAM to the direct radiative effect of increased CO_2 (Mutton et al. 2022), could help obtain a greater understanding of the mechanisms and processes that influence the WAM in the full response to increased CO_2. Previously in Mutton et al. (2022), it was found that in response to the direct radiative effect, the WAM precipitation increased. This increase was caused by a northward shift and weakening of the shallow meridional circulation over West Africa. The circulation changes were generated by large-scale changes in temperature as well as the local warming of the atmosphere caused by a soil moisture feedback over the Sahel. In contrast, in this paper, it was found that in response to a uniform ocean warming the WAM precipitation decreased. This decrease was caused (in part) by a strengthening of the shallow circulation over West Africa, again, with soil moisture feedbacks over the Sahel contributing to these circulation changes.

It is possible that the WAM coupled model response to increased CO_2 may be largely set by the differing magnitudes of the opposing effects of the direct radiative effect and the uniform ocean warming. It is also possible that the large spread in projections may be increased by the soil moisture feedback that acts to amplify any changes to the monsoon precipitation or circulation that occur. In future work we aim to understand how different models simulate the processes and mechanisms identified in these two papers. Examining intermodel differences could then help elucidate the source of the uncertainty in WAM projections in the coupled models as well as enabling analysis of possible emergent constraints. Previous work investigating intermodel differences in WAM projections has focused on future SST pattern changes such as Giannini et al. (2013); Park et al. (2015) and Park et al. (2016). Park et al. (2015) suggest that intermodel spread in Sahel rainfall projections can be largely explained through the difference in warming between tropical and extratropical SSTs in the Northern Hemisphere whilst Giannini et al. (2013) suggest the difference between North Atlantic SSTs and the global tropical SSTs is key to understanding WAM variability and intermodel differences in projections. Park et al. (2016) state that understanding Mediterranean Sea warming is key to understanding the

uncertainty in Sahel precipitation projections. The impact of a patterned SST change is another component of the Fig. 1 and timeslice precipitation decomposition and applying the results of Giannini et al. (2013); Park et al. (2015) and Park et al. (2016) to these experiments could provide valuable information.

Other methods have also been used previously to decompose WAM precipitation changes in a future climate. Monerie et al. (2021) decomposed precipitation changes into the fast response and the slow response, whereby the fast response refers to the effect of radiative warming over land and the slow response captures the effect of changes in ocean circulation. The work of Monerie et al. (2021) provides useful insight into the timescales over which the mechanisms identified in this paper or in Mutton et al. (2022) would be expected to occur.

Finally, a further path for future work could involve investigation into whether the findings in this paper relating to the WAM could also be applied to changes in other monsoon regions.

It is important to note a couple of limitations to the analysis presented in this paper. Firstly, the spin-up analysis is limited to the month of August since the model runs that we use only started on this month, and secondly, the spin-up analysis is limited to only one model. Despite this, the single model analysis allowed the use of experimental designs outside of the CMIP6 set, and enabled the identification of a set of mechanisms that have then then been investigated in other models from CMIP6. The analysis presented in this paper has provided insight into the different mechanisms acting to influence the WAM precipitation in response to a uniform ocean warming. The use of a spin-up experiment has allowed investigation into the causality of these different mechanisms and the timescales over which they occur, showing how the response progresses from the abrupt ocean warming to the long-term equilibrium response. Finally, through an analysis of the CMIP6 ensemble equilibrium response, it was shown that each of the mechanisms identified in the spin-up analysis may still be present in the equilibrium response.

Appendix 1: Figures 1 and 2 experiment description

Several CMIP6 experiments have been used to decompose the full forcing of CO_2 into different components as shown in Fig. 1. The coupled model column in Fig. 1 refers to the full forcing of increased CO_2 and is calculated by comparing years 50–150 of the piControl and Abrupt-4xCO2 CMIP6 experiments. This time frame was used to capture the slow response of the ocean warming as well as the direct radiative effect. The direct radiative effect refers to the impact of multiplying CO_2 concentrations by 4 whilst keeping SSTs unchanged. In Fig. 1, the impact of the direct radiative effect on the WAM has been calculated by comparing the amip and amip-4xCO2 experiments (two AGCM experiments forced by observed SSTs and atmospheric constituents, with the CO_2 concentrations multiplied by 4 in the case of the amip-4xCO2 experiment). The indirect effect of a uniform SST warming on the WAM has been calculated using the amip and amip-p4K experiment. Again, these experiments are two AGCM experiments forced by observed SSTs and atmospheric constituents, with a uniform warming of 4K applied in the case of amip-p4K. The future SST column in Fig. 1 refers to the impact of a uniform SST warming with an additional pattern applied, aiming to reflect a projected SST pattern in a future climate with increased atmospheric CO_2 concentrations. The amip and amip-future4K experiments were used here, where the SST pattern applied is calculated by taking a mean of the CMIP6 ensemble Abrupt-4xCO2 experiment. Similar to the amip-p4K experiment, in the amip-future4K experiment, CO_2 concentrations remain unchanged from the amip experiment.

Although these amip experiments described do provide useful insight the mechanisms seen in the direct radiative effect and uniform SST warming response, in order to produce an accurate decomposition of the full coupled model response to increased CO_2 the AGCMs used must be forced with SSTs from the associated coupled model. Such a decomposition can be made using the timeslice experiments used by Chadwick et al. (2017), which use SST forcing from each coupled model's own piControl and abrupt-4xCO2 experiment. The decomposition produced using these experiments uses a very similar framework to the amip based decomposition described previously but also includes further elements of the full forcing of increased CO_2 such as the plant physiological effect (i.e. the impact of changing plant physiology in response to increased CO_2) and the the impact of melting sea ice. The experiment set-up used to produce this decomposition is presented in Table 1 and the different components of the full response are calculated as stated in Table 2. The map plots presented in Fig. 2 show the sum of all the components, the coupled model response, and the difference between the two.

Appendix 2: Definition of key quantities

Mass weighted vertical average

A mass weighted vertical average has been calculated as.

$$\text{mass weighted vertical average} = \int_{p_b}^{p_a} x\,dp/(p_a - p_b) \quad (1)$$

Table 1 Description of experimental set-up for timeslice experiments used in Fig. 2

Timeslice experiments			
Experiment name	Prescribed SSTs	CO_2 concentrations	Sea ice
piSST	piControl	Pre-industrial	piControl
piSST-4xCO2-rad	piControl	Pre-industrial × 4 (only seen by the radiation scheme)	piControl
piSST-4xCO2	piControl	Pre-industrial × 4	piControl
piSST-pxK	piControl + mean global SST anomaly from abrupt-4xCO2 - piControl	Pre-industrial	piControl
a4SST	abrupt-4xCO2	Pre-industrial	piControl
a4SSTice	abrupt-4xCO2	Pre-industrial	abrupt-4xCO2

Each component of the full CO_2 forcing is calculated as described in Table 2

Table 2 Definition of components of full forcing of increased CO_2 using timeslice experiments

Timeslice component definition
Direct radiative effect = piSST-4xCO2-rad − piSST
Uniform SST warming = piSST-pxK − piSST
Patterned SST change = a4SST − piSST-pxK
Plant effect = piSST-4xCO2 − piSST-4xCO2-rad
Sea ice effect = a4SSTice − a4SST

where x represents the relevant variable being integrated (e.g. temperature), and p_a and p_b represent the top and bottom pressure limits of the integral.

Atmospheric moisture budget

A vertically integrated moisture budget has been calculated as.

$$\frac{\partial W}{\partial t} = E - P - \nabla \cdot Q \tag{2}$$

where $\frac{\partial W}{\partial t}$ is the rate of change of vertically integrated atmospheric moisture content, $\nabla \cdot Q$ is the vertically integrated moisture divergence, E is the evaporation, and P is the precipitation (Brown and Kummerow 2014; Trenberth et al. 2011).

Equivalent potential temperature

Equivalent potential temperature (θ_e) has been calculated as.

$$\theta_e = \left(T + \frac{L_v}{c_p} r\right)\left(\frac{p_0}{p}\right)^{\frac{R_d}{c_p}} \tag{3}$$

where T is the atmospheric temperature, L_v is the latent heat of vaporization, c_p is the specific heat capacity at constant pressure, p_0 is the standard reference pressure of 1000 hPa, p is the atmospheric pressure, and R_d is the specific gas constant (Stull 1988).

Horizontal divergences

Horizontal divergence of winds and horizontal divergence of moisture flux has been calculated as.

$$\text{Horizontal divergence of winds} = \nabla_h \cdot V \tag{4}$$

$$\text{Horizontal divergence of moisture flux} = \nabla_h \cdot qV \tag{5}$$

where V is the wind, and $\nabla_h \cdot$ is the horizontal divergence operator.

The change in horizontal divergence of moisture transport between amip and amip-p4K has been decomposed into dynamic and thermodynamic components (Endo and Kitoh 2014).

$$\Delta_{Dynamic}(\nabla_h \cdot qV) = \nabla_h \cdot (q_A \Delta V) \tag{6}$$

$$\Delta_{Thermodynamic}(\nabla_h \cdot qV) = \nabla_h \cdot (V_A \Delta q) \tag{7}$$

where subscripts A refer to the amip experiment and Δ refers to the difference between the amip-4xCO2 and amip experiments.

Low level atmospheric thickness (LLAT)

As defined by Lavaysse et al. (2009) and Shekhar and Boos (2017), Low Level Atmospheric Thickness (LLAT) has been calculated as.

$$\text{LLAT} = Z_g(700\,\text{hPa}) - Z_g(925\,\text{hPa}) \tag{8}$$

where $Z_g(x)$ is the geopotential height at pressure x. LLAT is used here to document changes in the shallow circulation over West Africa.

Acknowledgements Mat Collins, and F. Hugo Lambert were supported by NERC NE/S004645/1. Harry Mutton was supported by a PhD scholarship from the University of Exeter. Ruth Geen was supported by the UK-China Research & Innovation Partnership Fund, through the Met Office Climate Science for Service Partnership (CSSP) China, as part of the Newton Fund. Chris Taylor was supported by the African Monsoon Multidisciplinary Analysis-2050 project (Grant NE/M020428/1). The authors also thank the three anonymous reviewers who through their valuable feedback helped improve the manuscript greatly.

Author Contributions HM wrote the manuscript text and produced all figures with the direction of study devised alongside RC, MC, and HL. CT, RG and AT provided valuable feedback on numerous drafts and AT produced the model runs of the set of spin-up experiments used.

Funding Mat Collins, and F. Hugo Lambert were supported by NERC NE/S004645/1. Harry Mutton was supported by a PhD scholarship from the University of Exeter. Ruth Geen was supported by the UK-China Research & Innovation Partnership Fund, through the Met Office Climate Science for Service Partnership (CSSP) China, as part of the Newton Fund. Chris Taylor was supported by the African Monsoon Multidisciplinary Analysis-2050 project (Grant NE/M020428/1).

Availability of data and materials CMIP6 data was accessed from the ESGF CEDA data node https://esgf-index1.ceda.ac.uk/search/cmip6-ceda/. Data from the HadGEM2-A spin-up experiments are archived at the Met Office and available from the authors on request for research purposes.

Declarations

Conflict of interest The authors have no relevant financial or non-financial interests to disclose.

Ethical approval Not applicable.

References

Akinsanola AA, Zhou W (2020) Understanding the variability of west African summer monsoon rainfall: contrasting tropospheric features and monsoon index. Atmosphere. https://doi.org/10.3390/atmos11030309

Besson L, Lemaitre Y (2014) Mesoscale convective systems in relation to African and tropical easterly jets. Mon Weather Rev 142:3224–3242. https://doi.org/10.1175/MWR-D-13-00247.1

Biasutti M (2013) Forced Sahel rainfall trends in the cmip5 archive. J Geophys Res Atmos 118:1613–1623. https://doi.org/10.1002/jgrd.50206

Biasutti M (2019) Rainfall trends in the African Sahel: characteristics, processes, and causes. Wiley Interdiscipl Rev Clim Change. https://doi.org/10.1002/wcc.591

Brown P, Kummerow C (2014) An assessment of atmospheric water budget components over tropical oceans. J Clim 27:2054–2071. https://doi.org/10.1175/JCLI-D-13-00385.1

Busby JW, Cook KH, Vizy EK et al (2014) Identifying hot spots of security vulnerability associated with climate change in Africa. Clim Change 124:717–731. https://doi.org/10.1007/s10584-014-1142-z

Byrne M, O'Gorman P (2016) Understanding decreases in land relative humidity with global warming: conceptual model and GCM simulations. J Clim 29:9045–9061. https://doi.org/10.1175/JCLI-D-16-0351.1

Caminade C, Terray L (2010) Twentieth century Sahel rainfall variability as simulated by the arpege agcm, and future changes. Clim Dyn. https://doi.org/10.1007/s00382-009-0545-4

Chadwick R, Good P, Willett K (2016) A simple moisture advection model of specific humidity change over land in response to sst warming. J Clim 29:7613–7632. https://doi.org/10.1175/JCLI-D-16-0241.1

Chadwick R, Douville H, Skinner C (2017) Timeslice experiments for understanding regional climate projections: applications to the tropical hydrological cycle and European winter circulation. Clim Dyn. https://doi.org/10.1007/s00382-016-3488-6

Chadwick R, Ackerley D, Ogura T et al (2019) Separating the influences of land warming, the direct co 2 effect, the plant physiological effect, and sst warming on regional precipitation changes. J Geophys Res Atmos. https://doi.org/10.1029/2018JD029423

Cook KH (1999) Generation of the African easterly jet and its role in determining west African precipitation. J Clim 12:1165–1184. https://doi.org/10.1175/1520-0442(1999)012<1165:GOTAEJ>2.0.CO;2

Cook K, Vizy E (2019) Contemporary climate change of the African monsoon systems. Curr Clim Change Rep. https://doi.org/10.1007/s40641-019-00130-1

Emanuel KA, Neelin JD, Bretherton C (1994) On large-scale circulations in convecting atmospheres. Q J R Meteorol Soc 120:1111–1143. https://doi.org/10.1002/qj.49712051902

Endo H, Kitoh A (2014) Thermodynamic and dynamic effects on regional monsoon rainfall changes in a warmer climate. Geophys Res Lett 41:1704–1710. https://doi.org/10.1002/2013GL059158

Gaetani M, Flamant C, Bastin S et al (2017) West African monsoon dynamics and precipitation: the competition between global SST warming and co2 increase in cmip5 idealized simulations. Clim Dyn 48:1353–1373. https://doi.org/10.1007/s00382-016-3146-z

Giannini A (2010) Mechanisms of climate change in the semiarid African Sahel: the local view. J Clim 23:743–756. https://doi.org/10.1175/2009JCLI3123.1

Giannini A, Saravanan R, Chang P (2003) Oceanic forcing of Sahel rainfall on interannual to interdecadal time scales. Science 302:1027–1030. https://doi.org/10.1126/science.1089357

Giannini A, Biasutti M, Held I et al (2008) A global perspective on African climate. Clim Change 90:359–383. https://doi.org/10.1007/s10584-008-9396-y

Giannini A, Salack S, Lodoun T et al (2013) A unifying view of climate change in the Sahel linking intra-seasonal, interannual and longer time scales. Environ Res Lett. https://doi.org/10.1088/1748-9326/8/2/024010

He J, Soden BJ, Kirtman B (2014) The robustness of the atmospheric circulation and precipitation response to future anthropogenic surface warming. Geophys Res Lett 41:2614–2622. https://doi.org/10.1002/2014GL059435

Held IM, Soden B (2006) Robust responses of the hydrological cycle to global warming. J Clim 19:5686–5699. https://doi.org/10.1175/JCLI3990.1

Held IM, Delworth TL, Lu J et al (2005) Simulation of Sahel drought in the 20th and 21st centuries. PNAS 102:17891–17896. https://doi.org/10.1073/pnas.0509057102

Herceg D, Sobel A, Sun L (2007) Regional modeling of decadal rainfall variability over the Sahel. Clim Dyn 29:89–99. https://doi.org/10.1007/s00382-006-0218-5

Hill SA, Ming Y, Held IM et al (2017) A moist static energy budget-based analysis of the Sahel rainfall response to uniform oceanic warming. J Clim 30:5637–5660. https://doi.org/10.1175/JCLI-D-16-0785.1

Lavaysse C, Flamant C, Janicot S et al (2009) Seasonal evolution of the west African heat low: a climatological perspective. Clim Dyn 33:313–330. https://doi.org/10.1007/s00382-009-0553-4

Lohou F, Kergoat L, Guichard F et al (2014) Surface response to rain events throughout the west African monsoon. Atmos Chem Phys 14:3883–3898. https://doi.org/10.5194/acp-14-3883-2014

Martin GM, Bellouin N, Collins WJ et al (2011) The hadgem2 family of met office unified model climate configurations. Geosci Model Dev 4:723–757. https://doi.org/10.5194/gmd-4-723-2011

Masson-Delmotte V, Zhai P, Chen Y et al (2021) Working Group I contribution to the sixth assessment report of the intergovernmental panel on climate change. In: IPCC. https://doi.org/10.1017/9781009157896

Monerie PA, Sanchez-Gomez E, Gaetani M et al (2020) Future evolution of the Sahel precipitation zonal contrast in cesm1. Clim Dyn 55:2801–2821. https://doi.org/10.1007/s00382-020-05417-w

Monerie PA, Pohl B, Gaetani M (2021) The fast response of Sahel precipitation to climate change allows effective mitigation action. npj Clim Atmos Sci. https://doi.org/10.1038/s41612-021-00179-6

Mutton H, Chadwick R, Collins M et al (2022) The impact of the direct radiative effect of increased co2 on the west African monsoon. J Clim 35:2441–2458. https://doi.org/10.1175/JCLI-D-21-0340.1

Park JY, Bader J, Matei D (2015) Northern-hemispheric differential warming is the key to understanding the discrepancies in the projected Sahel rainfall. Nat Commun. https://doi.org/10.1038/ncomms6985

Park JY, Bader J, Matei D (2016) Anthropogenic Mediterranean warming essential driver for present and future Sahel rainfall. Nat Clim Chang 6:941–945. https://doi.org/10.1038/NCLIMATE3065

Raj J, Bangalath H, Stenchikov G (2019) West African monsoon: current state and future projections in a high-resolution AGCM. Clim Dyn 52:6441–6461. https://doi.org/10.1007/s00382-018-4522-7

Shekhar R, Boos W (2017) Weakening and shifting of the Saharan shallow meridional circulation during wet years of the west African monsoon. J Clim 30:7399–7422. https://doi.org/10.1175/JCLI-D-16-0696.s1

Skinner CB, Ashfaq M, Diffenbaugh NS (2012) Influence of twenty-first-century atmospheric and sea surface temperature forcing on west African climate. J Clim 25:527–542. https://doi.org/10.1175/2011JCLI4183.1

Sobel AH, Nilsson J, Polvani ML (2001) The weak temperature gradient approximation and balanced tropical moisture waves. J Atmos Sci 58:3650–3665. https://doi.org/10.1175/1520-0469(2001)058<3650:TWTGAA>2.0.CO;2

Stull RB (1988) An introduction to boundary layer meteorology. Kluwer Academic Publishers, Alphen aan den Rijn

Trenberth K, Fasullo J, Mackaro J (2011) Atmospheric moisture transports from ocean to land and global energy flows in reanalyses. J Clim 24:4907–4924. https://doi.org/10.1175/2011JCLI4171.1

Wang B, Ding Q (2006) Changes in global monsoon precipitation over the past 56 years. Geophys Res Lett. https://doi.org/10.1029/2005GL025347

Wang B, Biasutti M, Byrne MP et al (2020) Monsoons climate change assessment. Bull Am Meteorol Soc. https://doi.org/10.1175/bams-d-19-0335.1

Zhang G, Cook K (2014) West African monsoon demise: climatology, interannual variations, and relationship to seasonal rainfall. J Geophys Res 119:10175–10193. https://doi.org/10.1002/2014JD022043

Zhang G, Nolan DS, Thorncroft CD et al (2008) Shallow meridional circulations in the tropical atmosphere. J Clim 21:3453–3470. https://doi.org/10.1175/2007JCLI1870.1